ACS APPLIED MATERIALS & INTERFACES

www.acsami.org Research Article

Low-k SiO_x/AlO_x Nanolaminate Dielectric on Dielectric Achieved by Hybrid Pulsed Chemical Vapor Deposition

James Huang, Jing Mu, Yunil Cho, Charles Winter, Victor Wang, Zichen Zhang, Kesong Wang, Chanyoung Kim, Ajay Yadav, Keith Wong, Srinivas Nemani, Ellie Yieh, and Andrew Kummel*

Cite This: https://doi.org/10.1021/acsami.3c13973 Read Online

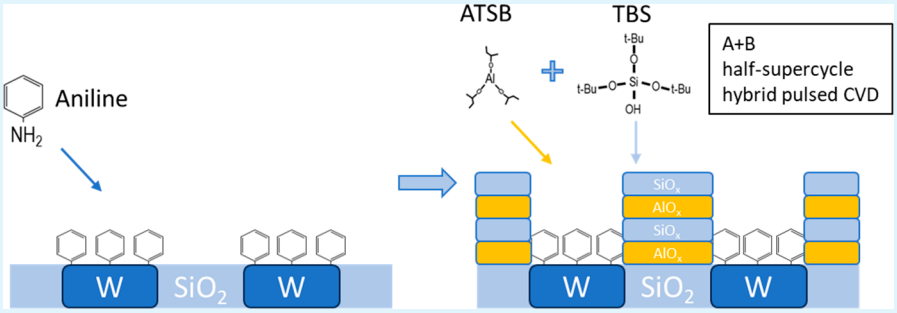

ABSTRACT: Selective and smooth low-k SiO_x/AlO_x nanolaminate dielectric on dielectric (DOD) was achieved by a hybrid water-free pulsed CVD process consisting of 50 pulses of ATSB (tris(2-butoxy)aluminum) at 330 °C and a 60 s TBS (tris(*tert*-butoxy)silanol) exposure at 200 °C. Aniline selective passivation was demonstrated on W surfaces in preference to Si_3N_4 and SiO_2 at 300 °C. At 200 °C, TBS pulsed CVD exhibited no growth on W or SiO_2, but its growth was catalyzed by AlO_x. Using a two-temperature pulsed CVD process, ~2.7 nm selective SiO_x/AlO_x nanolaminate was deposited on Si_3N_4 in preference to aniline passivated W. Nanoselectivity was confirmed and demonstrated on nanoscale W/SiO_2 patterned samples by TEM analysis. For a 1:1 Si:Al ratio, a dielectric constant (k) value of 3.3 was measured. For a 2:1 Si:Al ratio, a dielectric constant (k) value of 2.5 was measured. The k value well below that of Al_2O_3 and SiO_2 is consistent with the formation of a low-density, low-k SiO_2/Al_2O_3 nanolaminate in a purely thermal process. This is the first report of a further thermal CVD process for deposition of a low-k dielectric and the first report for a selective low-k process on the nanoscale.

KEYWORDS: *selective CVD, SiO_x, AlO_x, nanolaminate, dielectric on dielectric, low-k dielectric*

1. INTRODUCTION

The semiconductor industry continues scaling up three-dimensional integrated circuits (ICs). IC scaling is achieved by shrinking the sizes of the devices and interconnects. Shorter interconnect lengths improve the performance and reduce power consumption. However, continued scaling of ICs in the nanometer dimension results in interconnect misalignment. Interconnect misalignment leads to shorting and capacitive coupling between vias.[1] Chen et al. demonstrated that misalignment can be solved by dielectric on dielectric (DOD) deposition which selectively deposits a buffer layer of dielectric on the existing dielectric in preference to metal (schematic diagram shown in Figure 1).[1] The selective dielectric layer increases the distance (x' compared to x) between the misaligned via and the metal line distance, which improves shorting, capacitive coupling, and time-dependent dielectric breakdown (TDDB).

Selective DOD can be achieved by either atomic layer deposition (ALD) or chemical vapor deposition (CVD) with the help of small molecule inhibitors (SMI) as the metal passivant. Previously, Hashmi et al. and others used alkylphosphonic acid (octadecylphosphonic acid) or thiolate as the metal passivant to achieve ZnO and Al_2O_3 DOD;[2−4] however, no selectivity studies were conducted on nanoscale patterned samples with the octadecylphosphonic acid passivation.[2] Thiolate passivation only showed good selectivity on the blanket samples while poor selectivity and poor uniformity were observed on nanoscale patterned samples.[4] Both phosphonic acid and thiolate passivation require low-temperature atomic layer deposition which typically requires water as coreactant. The performance of back-end-of-line (BEOL) circuits could be compromised by these water-based ALD, as

Received: September 18, 2023
Revised: November 3, 2023
Accepted: November 6, 2023

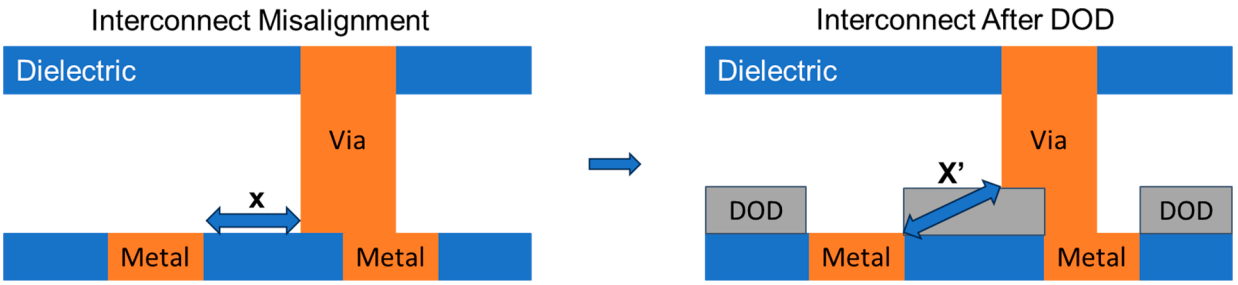

Figure 1. Schematic diagram of dielectric on dielectric (DOD) shows how it increases the distance between vias and metal lines by creating a metal recess. By utilizing DOD, interconnect misalignment effect can be effectively reduced, resulting in a larger via to metal line distance.

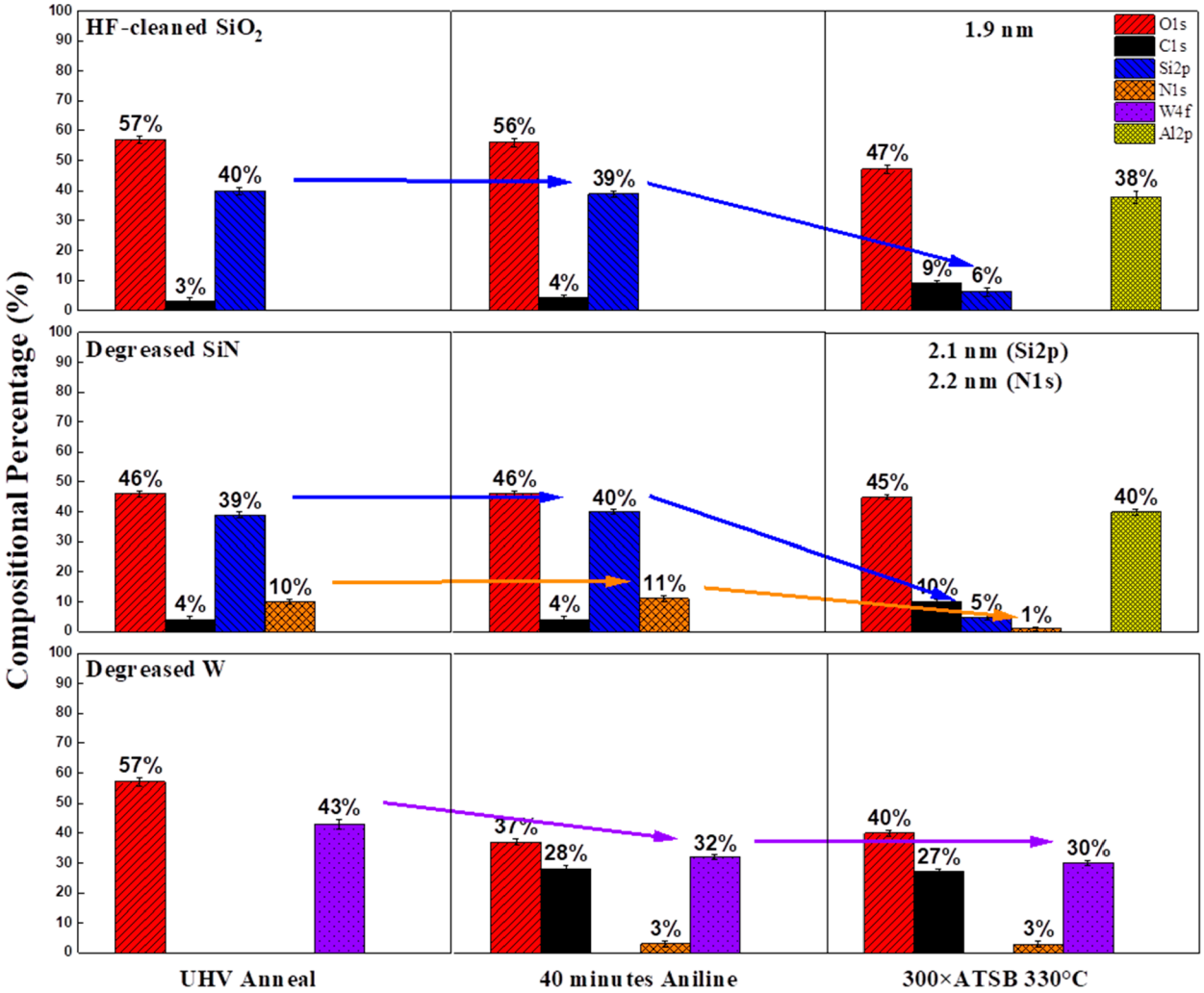

Figure 2. AlO_x growth on aniline passivated SiO_2, Si_3N_4, and W. 500 ms with a 10 s purge time of pulsed ATSB CVD at 330 °C. Raw data can be found in Figure S2.

a small quantity of water may introduce a substantial rise in the dielectric constant of porous low-*k* materials.

Short-chain small molecule inhibitors have been successfully used at high temperatures. Shearer et al. demonstrated a 3 nm selectivity of Al_2O_3 deposition on SiO_2 in preference to Cu using small molecule inhibitors such as pyrrole, aniline, and pyridine.[5] Merkx et al. showed a 6 nm selectivity TaN deposition on oxide (Al_2O_3/SiO_2) in preference to metal (Ru/Co) with aniline passivation at 250 °C with a plasma-enhanced ALD process.[6] However, this plasma TaN process is not suitable for BEOL DOD because photons, radicals, and ions from the plasma may damage the commonly used low-*k* material SiCOH.[7]

There are previous reports of 5 nm selective deposition of AlO_2, TiO_2, and HfO_2 on SiO_2 in preference to W with 300 °C aniline passivation.[8] These AlO_2, TiO_2, and HfO_2 DOD depositions were achieved by water-free pulsed CVD using tris(2-butoxy)aluminum (ATSB), hafnium *tert*-butoxide, and titanium isopropoxide, respectively.[9−11] In the present study, a "water-free process" denotes the absence of water as a coreactant; however, a minute quantity of water might be formed by dehydration reactions of the alkoxy precursor

https://doi.org/10.1021/acsami.3c13973
ACS Appl. Mater. Interfaces XXXX, XXX, XXX−XXX

ligands. Of these pulsed CVD selectively deposited DOD dielectric materials, Al_2O_3 (k = 7−8) had the lowest k value. Because lower dielectric constants can have reduced capacitive coupling, the exploration of a water-free low-k DOD process is imperative.

With a dielectric constant of 3.9, SiO_2 has an acceptable low-k value widely used in the semiconductor industry. There are three main types of processes used for SiO_2 deposition. Two of them either require extremely high CVD substrate temperature (>700 °C) or use water/plasma as the coreactant which are not compatible with the desired BEOL DOD application.[12−15] The catalytic-based ALD is the only SiO_2 process that does not involve the use of high temperature, water, or plasma. Numerous studies have been conducted on the catalytic-based SiO_2/Al_2O_3 nanolaminate with a k value close to 4.1, utilizing either TBS (tris(*tert*-butoxy)silanol) or TPS (tris(*tert*-pentoxy)silanol) together in combination with trimethylaluminum (catalyst TMA).[16−18] With an initial TMA pulse, TBS/TPS tends to decompose and form sequential SiO_2 nanolaminate layers. However, TMA tends to bond with oxygen and hydroxy sites on the surface. Consequently, it proves challenging to passivate against TMA substrate reactions with a small molecule inhibitor because TMA can readily displace SMI and form bonds with surface oxide (shown in Figure S1).[5] To date, there has been no reported selectivity study for the catalytically based SiO_2/Al_2O_3 ALD process.

In a previous study, pulsed CVD AlO_x DOD was successfully deposited on SiO_2 and not on the W surface.[8] By utilizing aniline passivation, ATSB alone proved capable of depositing up to 4 nm of selective DOD on SiO_2 surface at 330 °C.[8] This present report documents the benefits of merging the area-selective ATSB process with the low-k catalytic-based SiO_2/Al_2O_3 nanolaminate process. Through this combination, a selective low-k dielectric on dielectric can be achieved by using the novel hybrid two-temperature pulsed CVD leveraging the advantages of both techniques.

2. RESULTS AND DISCUSSION

2.1. Aniline Passivation and TBS Reactivity on Different Surfaces. In previous studies on water-free selective oxide deposition, water-free pulsed CVD has been shown to exhibit faster growth on metal surfaces compared to SiO_2.[8] This phenomenon is particularly evident on W metal surfaces, which tend to undergo oxidation. Because of this facile oxidation, W has a propensity to favor the formation of hydroxyl groups and oxide layers.[8] To inhibit oxide growth on metals and allow growth on dielectrics, aniline passivation is required. The passivation ability of aniline was tested on HF-cleaned SiO_2, degreased Si_3N_4, and degreased W substrates with the pulsed AlO_x (ATSB) CVD.

In Figure 2, the XPS chemical composition of HF-cleaned SiO_2, degreased Si_3N_4, and degreased W is shown at different stages of the process. This includes a 300 °C rapid UHV anneal, following a 40 min aniline passivation at 300 °C, and after pulsed CVD of AlO_x using ATSB as the single precursor. After aniline passivation, the C_{1s} signal from W increased from 0% to 28%, while the W_{4f} signal decreased from 42% to 32%. Both the Si_{2p} and C_{1s} signals from Si_3N_4 and SiO_2 remain unchanged. This indicates selective aniline passivation performed on the W in preference to SiO_2 and Si_3N_4.

As shown in Figure 2, after a total of 300 pulses of ATSB, around 1.9 and 2.2 nm of suboxide AlO_x was selectively deposited on SiO_2 and Si_3N_4, respectively; conversely, no deposition was observed on aniline passivated W. ATSB shows a similar, if not faster, growth rate on Si_3N_4 than SiO_2. Deposition thickness was derived from the equation between the inelastic mean free path and the Si_{2p} signal attenuation length of an electron from the substrate (method details shown in the Supporting Information Section S1).

When examining the Si_3N_4 substrate, the thickness derived from the N_{1s} signal was found to be similar to the thickness derived from the Si_{2p}. The similarity in the values derived from the N_{1s} and Si_{2p} signals suggests that both signals can be reliably used to estimate the thickness of the AlO_x layer on Si_3N_4. In the SiO_x/AlO_x nanolaminates (below), it is anticipated that the Si_{2p} signal from the nanolaminate will overlap with the signal from the SiO_2 substrate. Therefore, the focus of the subsequent session will primarily be on the selectivity of SiO_x/AlO_x nanolaminates on Si_3N_4 vs W because the N_{1s} signal can be used to quantify the deposition of SiO_x/AlO_x on this insulator.

To achieve selective deposition of SiO_x/AlO_x nanolaminates, TBS reactivity on Si_3N_4 and W was studied after aniline passivation. According to Figure 3, TBS at 250 °C

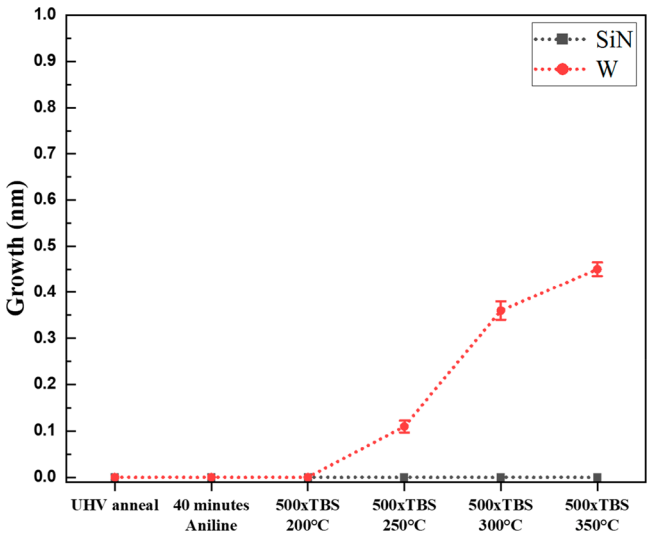

Figure 3. TBS reactivity test on Si_3N_4 vs aniline passivated W at various substrate temperatures. 500 ms pulse time with a 10 s purge time of pulsed TBS CVD. The XPS plot and raw data can be found in Figure S3.

exhibits a preference for depositing SiO_2 on the W surface rather than on the Si_3N_4. The observed results indicate two important findings. First, aniline is not effective in passivating TBS reactions, as TBS still exhibits reactivity toward aniline passivated W with the active silanol end group. Second, the presence of W/WO_x suggests that it may act as a Lewis acid site, facilitating the catalysis of the SiO_2 reaction, which promotes SiO_2 deposition on the W surface without the presence of TMA or ATSB at higher temperature (≥250 °C).[19]

The investigation of TBS reactivity was extended to different substrate temperatures (250−350 °C), revealing that a higher SiO_2 deposition rate was observed at elevated temperatures during the CVD process. This can be attributed to the decomposition of TBS and subsequent SiO_2 formation on the W surface at higher temperature. No reaction or SiO_2

https://doi.org/10.1021/acsami.3c13973
ACS Appl. Mater. Interfaces XXXX, XXX, XXX−XXX

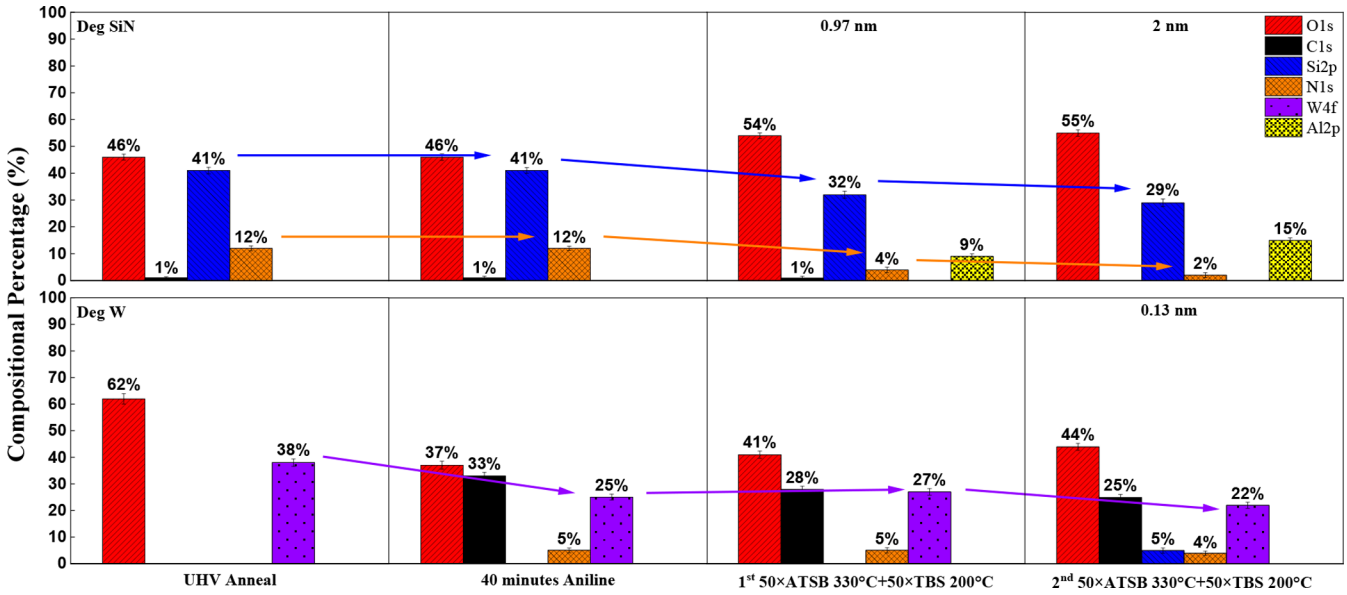

Figure 4. Pulsed ATSB at 330 °C followed by pulsed TBS at 200 °C on Si_3N_4 vs aniline passivated W. The process utilized 50 pulses of ATSB at 330 °C and 50 pulses of TBS dosing at 200 °C. Both ATSB and TBS have a pulse time of 500 ms and a 10 s purge time. The scatter plot and raw data can be found in Figure S5.

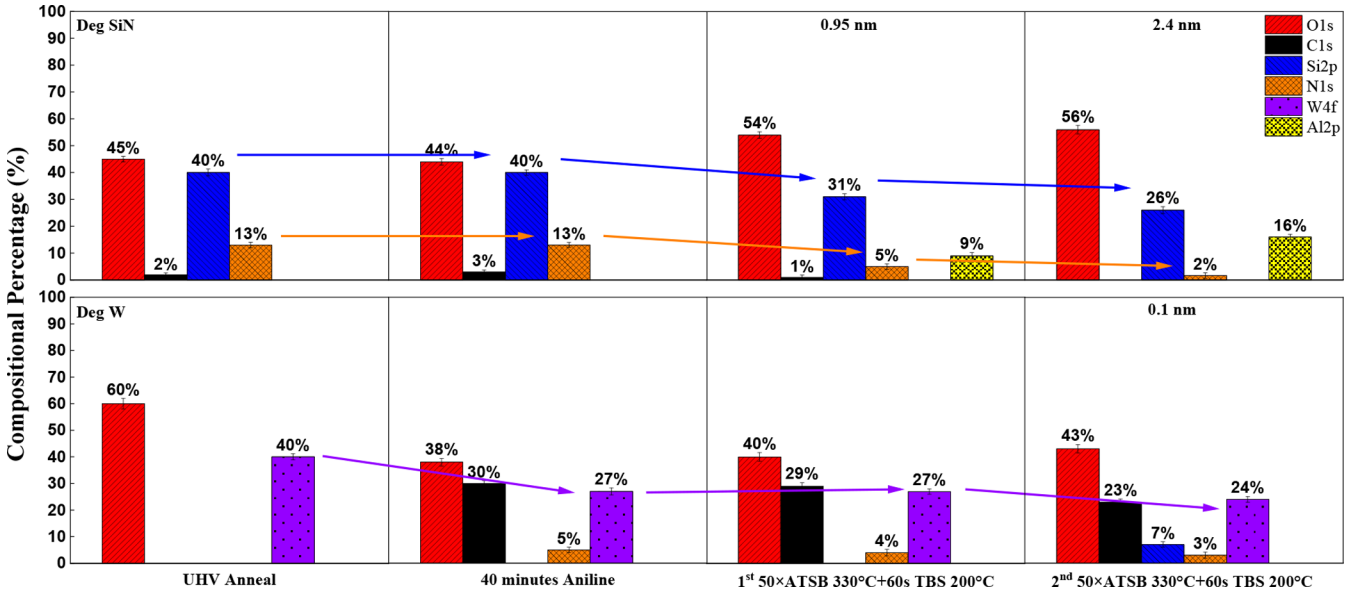

Figure 5. Pulsed ATSB at 330 °C followed by continuous TBS exposure at 200 °C on Si_3N_4 vs aniline passivated W. The process utilized 50 pulses of ATSB at 330 °C and a 60 s continuous TBS at 200 °C. ATSB has a pulse time of 500 ms and a 10 s purge time. The scatter plot and raw data can be found in Figure S6.

deposition was observed on the aniline passivated W surface in the absence of Al at 200 °C. A single 60 s TBS exposure was studied on a Si_3N_4 and an aniline passivated W surface; XPS results proved that TBS became unreactive in the absence of Al at 200 °C on the aniline passivated W (XPS shown in Figure S4).

In summary, the substrate temperature during TBS dosing should be set equal to or below 200 °C to ensure the SiO_2 deposition is prevented on the W surface, allowing for the desired area selective SiO_x/AlO_x nanolaminates. At 200 °C TBS does not react with W; therefore, TBS selective reaction can be enabled through the catalytic reaction of TBS with the selectively deposited AlO_x on SiO_2/Si_3N_4.

2.2. SiO_x/AlO_x Nanolaminate Selectivity Optimization. Because the selectivity of AlO_x deposition using ATSB was optimized at 330 °C and TBS showed no deposition by itself at 200 °C, deposition with 50 pulses of ATSB at 330 °C followed by a 30 min purge and 50 pulses of TBS at 200 °C was performed on degreased Si_3N_4 and W (shown in Figure 4).

As shown in Figure 3, after the aniline passivation, the C_{1s} peak from W increased from 0% to 33%, the peak of O_{1s} decreased from 62% down to 37%, and no compositional signal changed on Si_3N_4. After the initial supercycle with the binary substrate temperature, around 0.97 nm was selectively deposited on Si_3N_4 while no deposition on W. The observed decrease in the C_{1s} signal from 33% to 28% and the increase in the O_{1s} signal from 37% to 41% on W suggested that the initial

https://doi.org/10.1021/acsami.3c13973
ACS Appl. Mater. Interfaces XXXX, XXX, XXX−XXX

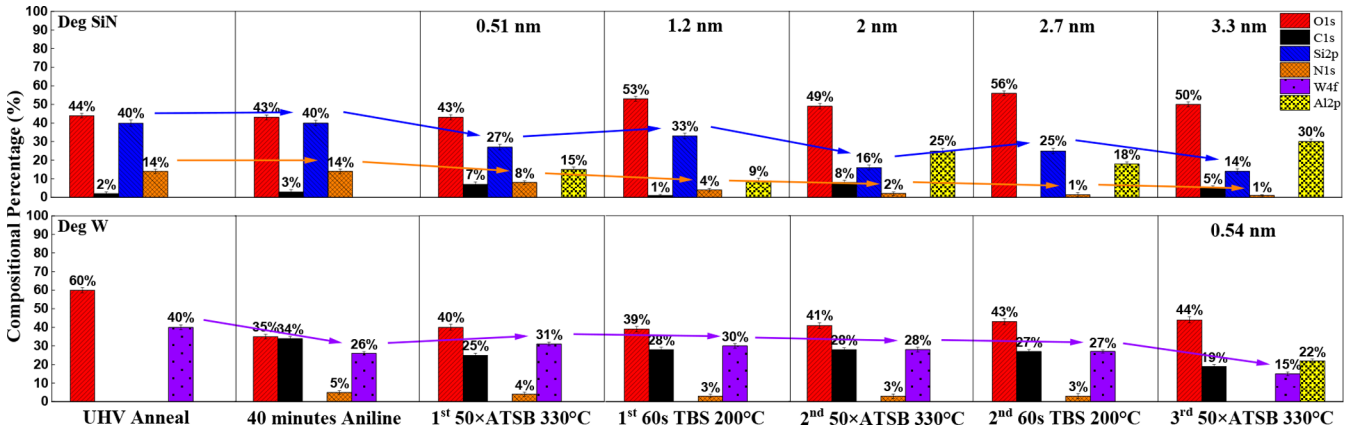

Figure 6. Half-supercycle hybrid pulsed ATSB at 330 °C with half-supercycle continuous TBS exposure at 200 °C on Si_3N_4 vs aniline passivated W. The process utilized 50 pulses of ATSB at 330 °C and a 60 s continuous TBS at 200 °C. ATSB has a pulse time of 500 ms and a 10 s purge time. The scatter plot and raw data can be found in Figure S7.

catalytic reaction of the SiO_x/AlO_x nanolaminate compromised the aniline passivation layer by introducing hydroxyl groups. The hydroxyl groups were probably originated from trace TBS silanol groups and released as a byproduct during the catalytic reaction. With an additional supercycle, around 2 nm of SiO_x/AlO_x was deposited on Si_3N_4 while only 0.13 nm was on W.

The deposition of 50 pulses of TBS requires approximately 9 min to complete. This extended dosing time increases the likelihood of compromising the aniline layer by introducing physiosorbed or chemisorbed hydroxyl species. According to previous research, the SiO_2 laminate growth depends on two competing factors: propagation/insertion and cross-linking.[18,20] Rapid TBS insertion promotes higher growth rates, while the occurrence of cross-linking inhibits the growth. During the initial few pulses of TBS, the SiO_2 layer can undergo cross-linking, effectively halting further growth. Subsequent pulses primarily compromise the integrity of the aniline layer rather than contribute to the growth process. Additionally, pulsing TBS does not enhance selectivity by purging physiosorbed TBS on the W surface due to its inert behavior in the absence of ATSB at 200 °C. Thus, 50 pulses of ATSB at 330 °C followed by 60 s continuous TBS exposure at 200 °C was performed on degreased Si_3N_4 and W (shown in Figure 5). As before, a 30 min purge was conducted between two precursors.

The XPS chemical composition analysis in Figure 5 demonstrated that after the first supercycle, the O_{1s} signal increased to 39% while the C_{1s} signal only decreased to 29%. This indicated that reducing the dosing time resulted in less damage to the aniline layer. After a second supercycle, this recipe achieved a higher selectivity of 2.4 nm of SiO_x/AlO_x deposition on Si_3N_4 in preference to W.

The longer pumping time for pressure recovery and higher residual pressure observed after TBS dosing, in comparison to ATSB, suggested that physiosorbed TBS on the chamber walls might slowly degas even after the dosing process is completed. Therefore, during the purging time between ATSB dosing and TBS dosing, TBS from the chamber walls might continue attacking the aniline passivation layer and result in an early loss of selectivity. The prolonged exposure of TBS during the purging time increased the likelihood of SiO_2 deposition on the W surface, utilizing W/WO_x as the Lewis acid catalytic sites. This explains the presence of a Si_{2p} signal (5%−7%) on W without Al_{2p} after the second supercycle.

A half-supercycle consisting of 50 pulses of ATSB CVD at 330 °C followed by an immediate XPS study was conducted. Subsequently, another half-supercycle involving a 60 s exposure to TBS at 200 °C was performed for further investigation.

As shown by the XPS study in Figure 6, each half-cycle process contributed around a monolayer thickness of the AlO_x or SiO_x interlayer, resulting in the formation of a nanolaminate structure. Around 2.7 nm of selective SiO_x/AlO_x deposition was deposited only on degreased Si_3N_4. Atomic force microscopy (AFM) measurement showed a smooth deposition with an RMS roughness of 0.8 nm (shown in Figure S8). By moving the sample back to the UHV chamber for XPS after each half-supercycle, no Si_{2p} signal was detected after the second round of the TBS dosing. However, during the subsequent 50 pulses of the ATSB half-supercycle, selectivity was lost, and approximately 0.54 nm of pure AlO_x was deposited on the W. This can be attributed to the high hydroxyl content and the decrease in aniline passivation on the W surface. Introducing TBS resulted in a selectivity loss of approximately 2 nm compared to the pure pulsed ATSB CCVD process described in the previous research.[9]

The hybrid half-supercycle process with a lower TBS dosing substrate temperature at 150 °C was investigated, along with a similar half-supercycle process involving a 120 s TBS dosing at the same temperature. The XPS chemical composition charts for these experiments can be found in Figures S9 and S10. Lowering the TBS dosing temperature allows for a higher number of half-supercycles to be dosed. Despite a slightly lower half-supercycle TBS growth rate, similar selectivity was achieved compared with the previous conditions. From Figure S10, longer half-supercycle TBS dosing (120 s) did not significantly impact selectivity. The increase in the TBS dosing time did not result in an increase in SiO_2 laminate growth. This suggests that the 60 s half-supercycle TBS is saturated and does not compromise aniline passivation.

The effect of ATSB thickness on selectivity was also examined by altering the number of ATSB pulses per half-supercycle while keeping the TBS dosing at 60 s and the temperature at 200 °C. Figures S11 and S12 depict the study conducted with lower (25 pulses) and higher (100 pulses) number of ATSB pulses, respectively. Both experiments

https://doi.org/10.1021/acsami.3c13973
ACS Appl. Mater. Interfaces XXXX, XXX, XXX−XXX

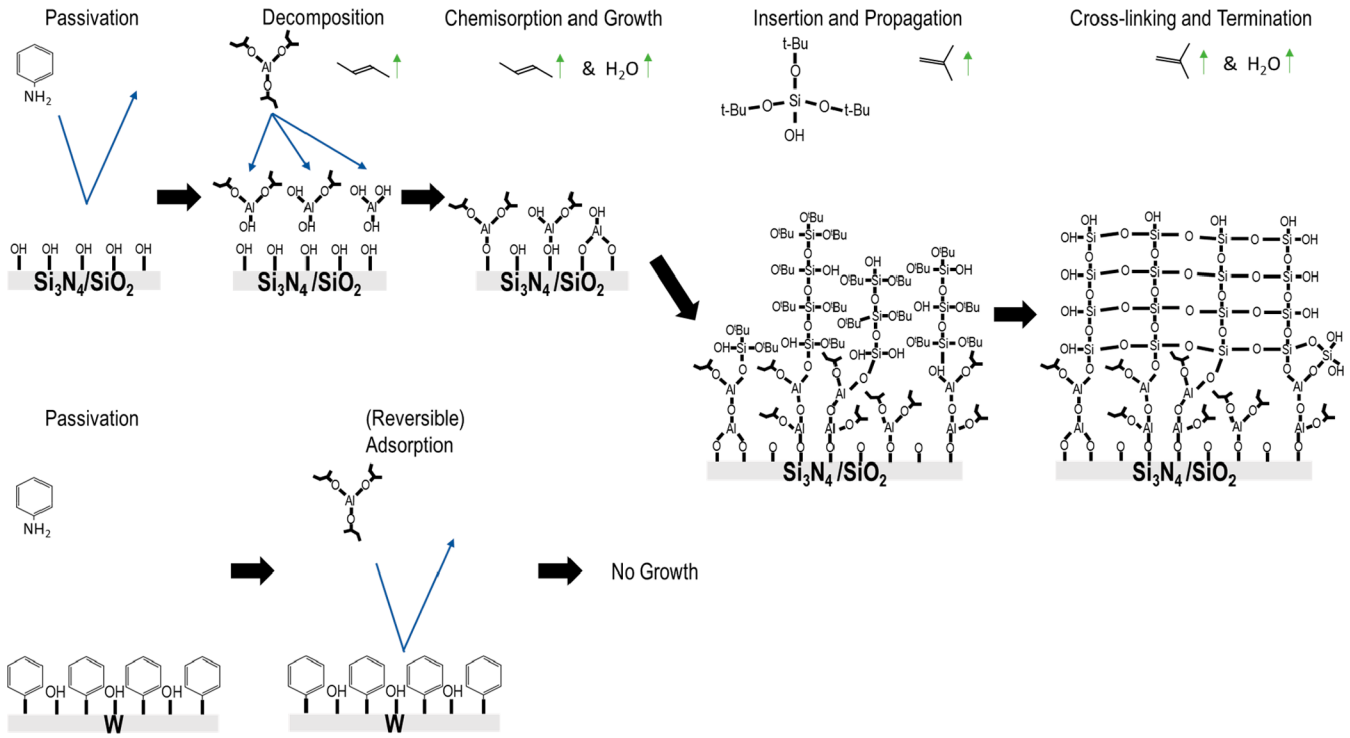

Figure 7. Proposed mechanism of hybrid half-supercycle pulsed CVD process on Si_3N_4/SiO_2 preferent to W with aniline passivation.

showed lower selectivity than the process shown in Figure 6. The results indicate that a lower number of ATSB pulses results in lower selectivity due to the formation of thinner AlO_x layers, while TBS remains the dominant factor contributing to the loss in selectivity. Conversely, with a higher number of ATSB pulses, the deposition of thicker ATSB layers leads to a loss in selectivity.

Tris(*tert*-pentoxy)silanol (TPS) is a common alternative precursor for SiO_x/AlO_x deposition. The half-supercycle process involving 50 pulses ATSB at 330 °C and 60 s TPS at 150 °C was also studied (shown in Figure S13). The XPS chemical compositional chart showed a selectivity of 1.6 nm SiO_x/AlO_x achieved on Si_3N_4 in preference to aniline passivated W. During the second-round half-supercycle TPS dosing, around 0.3 nm of pure SiO_2 was deposited on the W surface. This early loss in selectivity might be due to the higher reactivity of liquid phase TPS compared to solid phase TBS. Burton et al. demonstrated this increased reactivity by showing that TPS exhibits a substantially higher growth rate than TBS.[18] After thorough optimization efforts, the highest observed selectivity achieved is 2.7 nm using the hybrid half-supercycle process involving 50 pulses of ATSB at 330 °C and a 60 s TBS dosing at 200 °C.

2.3. SiO_x/AlO_x Nanolaminates Nanoselectivity and Capacitance−Voltage Measurement. A proposed mechanism of the hybrid half-supercycle pulsed CVD process with aniline passivation is shown in Figure 7. Because of the long duration of air exposure, there are Si−OH groups generated on the Si_3N_4 substrate surface. The aniline selectively passivates the W surface through W−C bonds (horizontal configuration) and W−N bonds (vertical configuration), while leaving Si_3N_4/SiO_2 unaffected. The detailed selective bonding of aniline to a metal surface has been previously studied by Tezsevin et al.[21] The hydrophobic phenyl ring and steric shielding of the aniline layer prevent the initial ATSB precursor from chemisorbing on W, causing it to physisorb only weakly and subsequently desorb at 330 °C.

The ATSB precursor decomposes when it physisorbs on the 330 °C Si_3N_4/SiO_2 substrate surface; a 2-butene byproduct desorbs, generating $Al(OH)(O{-}secBu)_2$, $Al(OH)_2(O{-}secBu)$, and maybe even some $Al(OH)_3$ species. Based on the low growth rate (~0.01 nm per ATSB cycle), ATSB most likely decomposed into $Al(OH)(O{-}secBu)_2$ or $Al(OH)_2(O{-}secBu)$. The presence of carbon associated with the O−*sec*-butyl ligands was confirmed through the previous XPS studies shown in Figure 6. $Al(OH)(O{-}secBu)_2$, $Al(OH)_2(O{-}secBu)$, and $Al(OH)_3$ can chemisorb on the Si_3N_4/SiO_2 surfaces by reacting with a surface isolated hydroxyl site or two adjacent hydroxyl sites. Given that the pK_a of surface Si−OH groups is 4.5, the pK_a of $Al(OH)_3$ is 11.2, and the pK_a of the CH_3CH_2OH ligand (similar to *sec*-butanol groups) is 15.9, protonation of Al−OH and Al−OR (Al−O−*sec*Bu) groups by the more acidic Si−OH groups is favorable during the chemisorption process.[22−24] The possible chemical reactions of the Si−OH groups with the Al−OH and Al−OR groups are shown in eqs 1 and 2. Additional hydroxyl groups from $Al(OH)_2(O{-}secBu)$ and $Al(OH)_3$ species allow continuous growth for subsequent pulses.

$$\mathrm{SI{-}OH(surface)} + \mathrm{Al{-}OH} \rightarrow \mathrm{Si{-}O{-}Al} + \mathrm{H_2O}\uparrow \quad (1)$$

$$\mathrm{Si{-}OH(surface)} + \mathrm{Al{-}OR} \rightarrow \mathrm{Si{-}O{-}Al} + \mathrm{ROH}\uparrow \quad (2)$$

For the second half-supercycle, the 60 s TBS dosing only reacts with the deposited AlO_x initial layer. With a pK_a of 10 for H_3SiO_3 and 11.2 for $Al(OH)_3$, the protonation reaction illustrated in eq 3 is favorable.[25]

$$\mathrm{Al{-}OH(surface)} + \mathrm{(RO)_3Si{-}OH} \rightarrow \mathrm{Al{-}O{-}Si(OR)_3} + \mathrm{H_2O}\uparrow \quad (3)$$

Equation 3 demonstrates that TBS (TPS) might undergo protonation with the Al−OH group to form $Al{-}O{-}Si(O^tBu)_3$.

https://doi.org/10.1021/acsami.3c13973
ACS Appl. Mater. Interfaces XXXX, XXX, XXX−XXX

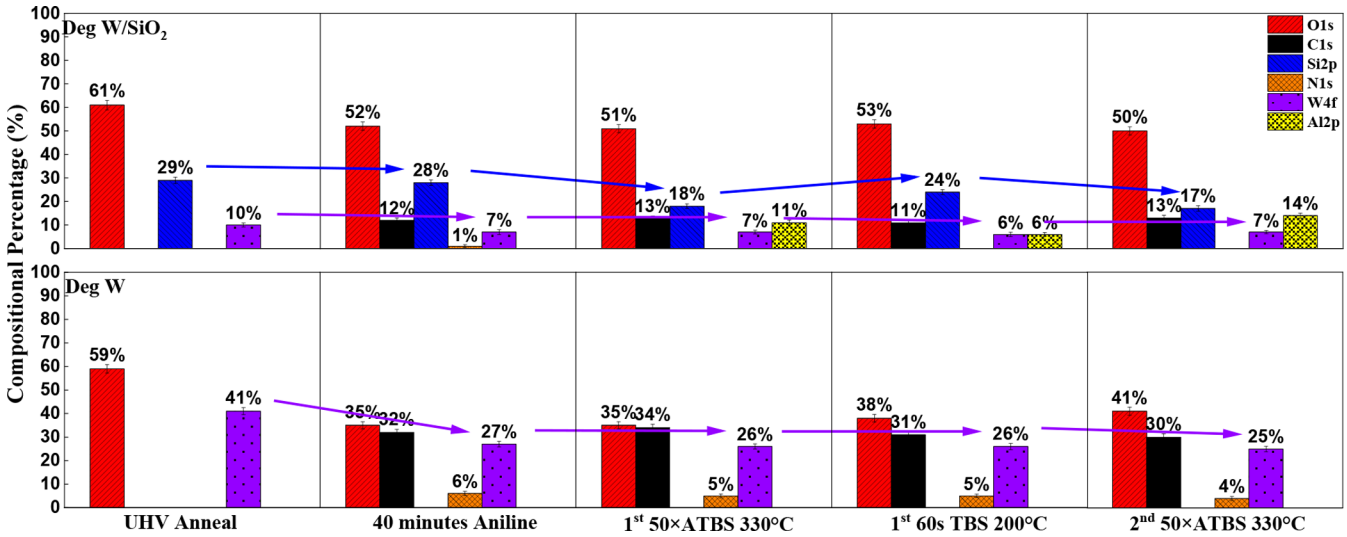

Figure 8. Selective hybrid pulsed SiO_x/AlO_x CVD on the SiO_2 region of the W/SiO_2 patterned sample with aniline passivation. The process utilized 50 pulses of ATSB at 330 °C and a 60 s TBS dosing at 200 °C. Raw data can be found in Figure S14.

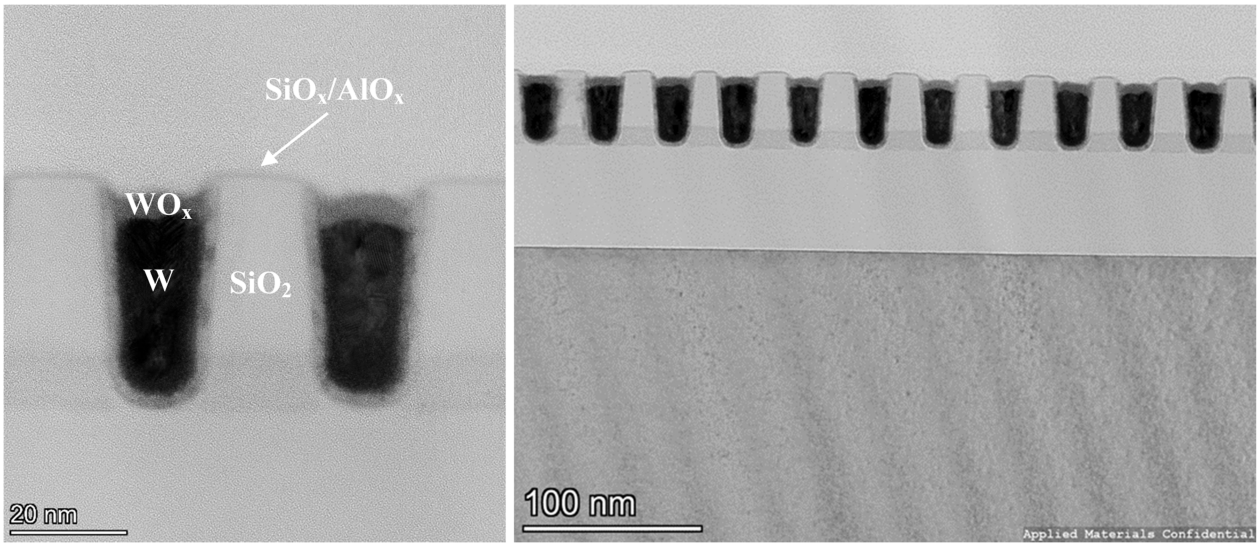

Figure 9. TEM images of the selective hybrid pulsed SiO_x/AlO_x CVD on SiO_2 region of W/SiO_2 patterned sample. The process utilized 50 pulses of ATSB at 330 °C and a 60 s TBS dosing at 200 °C. The EELS study is shown in Figure S15.

Moreover, TBS might also undergo protonation with Al−O−*sec*Bu groups, resulting in the formation of Al−O−Si(O^tBu)$_3$ with the release of HO−*sec*Bu ligands.

Additional TBS molecules will be subjected to Al−O−Si(O^tBu)$_2$−O−Si(O^tBu)$_3$ polymerization and release HO^tBu as the byproduct. A general chemical equation for this step is depicted in eq 4.

$$\text{Si–OR(surface)} + (\text{RO})_3\text{Si–OH} \rightarrow \text{Si–O–Si(OR)}_3 + \text{ROH}\uparrow \quad (4)$$

The remaining Si−O^tBu groups undergo 2-methylpropene group loss and lead to the formation of Si−OH bonds.[25] These Si−OH can then cross-link to form Si−O−Si bonds and emit water (shown in eqs 5 and 6, where R′ = alkene derived from the starting R group in eq 5).

$$\text{Si–OR} \rightarrow \text{Si–OH} + \text{R}'\uparrow \quad (5)$$

$$\text{Si–OH} + \text{Si–OH} \rightarrow \text{Si–O–Si} + \text{H}_2\text{O}\uparrow \quad (6)$$

Once Si−O−Si cross-linking bonds reach approximately a monolayer thickness (∼0.5 nm), TBS (TPS) can no longer come into proximity to the AlO_x layer and become harder to be protonated. This hindered proximity ultimately results in the termination of the reaction. Additionally, the presence of an excess number of O−*sec*-butyl groups branching out from the Al center results in a significant incorporation of carbon into the deposition film, and the film exhibits high porosity. The combination of a high carbon content and a high level of porosity leads to the formation of a low-*k* dielectric film.

The optimized hybrid half-supercycle process, utilizing 50 pulses of ATSB at 330 °C and a 60 s TBS dosing at 200 °C, demonstrated the highest observed selectivity of 2.7 nm. The same process was applied on a nanoscale W/SiO_2 patterned sample with a pitch size of 55 nm and a line width of 30 nm. By conducting the optimized hybrid pulsed CVD SiO_x/AlO_x process on the patterned sample, we quantified selectivity at the nanoscale level.

https://doi.org/10.1021/acsami.3c13973
ACS Appl. Mater. Interfaces XXXX, XXX, XXX−XXX

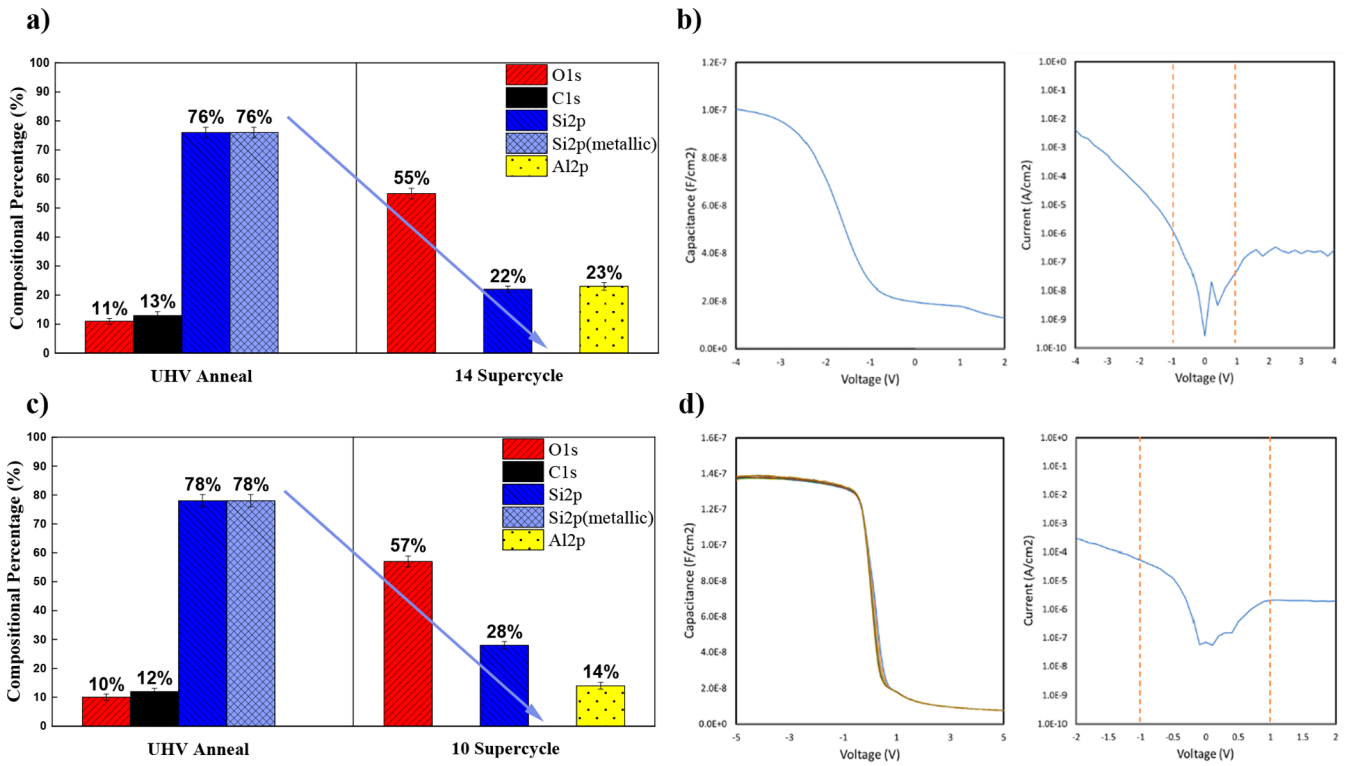

Figure 10. (a) Selective hybrid pulsed SiO_x/AlO_x CVD on Si for capacitance study. Fourteen supercycles of 50 pulses of ATSB at 330 °C and a 60 s TBS dosing at 200 °C were employed. Raw data can be found in Figure S16. (b) *CV* and *IV* measurement of the selective hybrid pulsed SiO_x/AlO_x CVD on Si. (c) Selective hybrid pulsed SiO_x/AlO_x CVD on Si for capacitance study. Ten supercycles of 25 pulses of ATSB at 330 °C and a 60 s TBS dosing at 200 °C were employed. Raw data can be found in Figure S17. (d) *CV* and *IV* measurement of the selective hybrid pulsed SiO_x/AlO_x CVD on Si with the 25 pulses of ATSB at 330 °C and a 60 s TBS dosing at 200 °C process.

In Figure 8, XPS analysis was performed during the hybrid pulsed SiO_x/AlO_x CVD on both the W/SiO_2 patterned sample and the blanket W sample. Initially, no carbon content was detected on the surface of either sample. After a 40 min aniline passivation step, the patterned surface exhibited approximately 12% carbon content, while the blanket W showed a monolayer of aniline passivation. The process was stopped after the second round of the ATSB half-supercycle to prevent overgrowth on the W region of the patterned sample. Following the initial ATSB half-supercycle, the Si_{2p} signal from the patterned sample decreased from 28% to 18%, and the Al_{2p} signal increased from 0% to 11%. The W_{4f} signal remained unchanged. Subsequently, during the TBS half-supercycle, the Si_{2p} signal from the patterned sample increased from 18% to 24%, indicating the deposition of SiO_2, while the Al_{2p} signal decreased from 11% to 6%. Lastly, samples were finished with another half-supercycle of ATSB.

TEM analysis was conducted on the W/SiO_2 patterned sample after deposition, as depicted in Figure 9. The images showed a SiO_x/AlO_x deposition of approximately 2 nm on the SiO_2 surface, while the W surface remained pristine.

To ensure the deposition of a thick and nonleaky SiO_x/AlO_x film suitable for capacitance−voltage (*CV*) and current−voltage (*IV*) study, 14 supercycles of the same deposition recipe (50 pulses of ATSB at 330 °C and a 60 s TBS dosing at 200 °C) were applied to a HF-cleaned Si substrate. From Figure 10a, the XPS data showed a 1:1 Si:Al ratio after the deposition. The as-deposited SiO_x/AlO_x thickness was measured to be approximately 29.3 nm by ellipsometry. Subsequently, a 30 min 450 °C O_2 anneal was performed, followed by a stepped forming gas anneal at 330, 350, and 380 °C for 15 min each. After these annealing steps, the thickness of the SiO_x/AlO_x deposition was reduced to around 28 nm. For electrical contact, the backside of the Si substrate was coated with sputtered gold, and a nickel dot electrode with a diameter of 145 μm was deposited. A separate HF-cleaned Si substrate−sample was dosed with 10 supercycles following the identical deposition recipe involving 50 pulses of ATSB at 330 °C and a 60 s TBS dosing at 200 °C. This sample underwent identical annealing procedures and Ni dot deposition. Subsequently, cross-sectional TEM analysis was performed to confirm that the deposition thickness observed matched the ellipsometry thickness measurement. In the TEM image Figure S18, a nanolaminate structure was clearly observed.

Figure 10b presents the single-frequency 1 MHz *CV* and *IV* measurements conducted on the deposited SiO_x/AlO_x film. Based on the measurements of capacitance, area, and thickness, the dielectric constant (k) value was calculated, yielding a value of 3.3. This low k value achieved by the SiO_x/AlO_x nanolaminate could be due to high porosity and carbon incorporation in the deposition film. The catalytic growth of SiO_2 using TBS involves two competing factors: insertion and cross-linking. Fast insertion combined with rapid cross-linking can potentially lead to a disordered arrangement of molecules and increased porosity in the SiO_2 interlayer. Furthermore, the *IV* measurement showed that within the voltage range of ±1 V, the current was measured to be less than or equal to 1×10^{-6} A/cm^2, indicating low leakage current, valid *CV* measurement, and satisfactory electrical properties of the deposited film for BEOL DOD application.

Author: Ten supercycles of the 25 pulses of ATSB at 330 °C and a 60 s TBS dosing at 200 °C were also performed on a

https://doi.org/10.1021/acsami.3c13973
ACS Appl. Mater. Interfaces XXXX, XXX, XXX−XXX

HF-cleaned Si to study the effect of Si ratio in the SiO_x/AlO_x nanolaminate on the CV performance. From Figure 10c, 25 pulses of ATSB at 330 °C and a 60 s TBS dosing at 200 °C process rendered a 2:1 Si:Al ratio. The as-deposited SiO_x/AlO_x thickness was measured to be approximately 15.7 nm by ellipsometry. The sample underwent a 30 min, 450 °C O_2 anneal, followed by a stepped forming gas anneal at 330, 350, and 380 °C for 15 min each. After these annealing steps, the thickness of the deposition became 15.6 nm. The backside of the sample was sputtered with gold, and a nickel dot electrode with a diameter of 145 μm was deposited on the deposition surface.

In Figure 10d, the multifrequency *CV* measurement and *IV* measurement were conducted on the deposited SiO_x/AlO_x film with a 25-pulse ATSB process to study the effect of frequency on the *CV* and calculate its *k* value. A minor frequency dependent *CV* shift was observed in the depletion region. This minimal frequency dependent *CV* shift would not affect the intended use of the film for the DOD application. Based on the measured capacitance, area, and thickness, the *k* value was calculated to be 2.5. The *IV* measurement of this thinner SiO_x/AlO_x nanolaminate showed a leakage current less than or equal to 1×10^{-4} A/cm^2 within the voltage range of ±1 V, indicating low leakage current and valid CV measurement. The rise in leakage current observed in this 2:1 Si:Al ratio sample in comparison to the Si:Al ratio of the 1:1 sample in Figure 10b is primarily attributed to the reduction in thickness. Nonetheless, it should be noted that the nanolaminates tend to absorb water from the atmosphere, leading to an increase in the *k* value up to 4.3 (2:1 Si:Al ratio shown in Figure S19) and 5 (1:1 Si:Al ratio shown in Figure S20). With additional UHV anneal, the *k* value of 2.5 of the 2:1 Si:Al ratio nanolaminate could be restored by extracting the water molecules out (shown in Figure S21). This indicates that further carbon incorporation may be needed to make the film more hydrophobic, or a simple encapsulation may be required to inhibit water adsorption.

3. CONCLUSION

A novel approach combining the selectivity of the pulsed ATSB CVD process with catalytic reactions using TBS/TPS was employed to achieve a low-*k* dielectric deposition for DOD applications. Aniline demonstrated selective passivation of the W surface over SiO_2 and Si_3N_4. TBS exhibited no growth in the absence of ATSB below or at 200 °C, preventing deposition in the absence of AlO_x. However, prolonged exposure to TBS could potentially compromise the aniline passivation layer by introducing hydroxyl groups. Additionally, the data are consistent with TBS utilizing W/WO_x as a Lewis acid site for catalyzing the SiO_2 reaction, leading to an early loss in selectivity compared to the pulsed AlO_x (ATSB) CVD. By incorporating aniline passivation and employing a hybrid half-cycle process involving 50 pulses of ATSB at 330 °C followed by a 60 s TBS exposure, a selective SiO_x/AlO_x nanolaminate with a thickness of approximately 2.7 nm was successfully deposited on Si_3N_4 while preserving a clean W surface. The same process was also applied to a nanoscale W/SiO_2 patterned substrate, resulting in a selective deposition of approximately 2 nm on SiO_2 only, as confirmed by TEM analysis. *CV* and *IV* measurements validated the ability of this process to deposit a low-*k* dielectric nanolaminate with a dielectric constant (*k*) value of 3.3 with a 1:1 Si:Al ratio and a *k* value of 2.5 with a 2:1 Si:Al ratio. The lower *k* value measured compared with pure SiO_2 can be attributed to the presence of porous SiO_2 interlayers. This is the first report of a further thermal CVD process for deposition of a low-*k* dielectric and the first report for a selective low-*k* process on the nanoscale.

4. METHODS

4.1. Reactor. A custom-built vacuum chamber system was utilized for all passivation, CVD processes, and deposition characterization (see chamber schematic diagram in Figure S22). The system consisted of three main chambers: the load-lock chamber (for sample loading and unloading), the deposition chamber, and the ultrahigh-vacuum (UHV) chamber. To facilitate a direct selectivity comparison, two or three samples were loaded simultaneously into the load-lock chamber.

The deposition chamber, which maintained a base pressure of 2×10^{-6} Torr, served as the primary space for all passivation and CVD experiments. It was equipped with a Pfeiffer TPH060 turbo pump and an Edwards RV3 rotary backing pump for effective evacuation. Samples were affixed to a copper sample block on a manipulator with a cartridge heater. During the passivation and CVD processes, samples were heated and positioned in the center of the deposition chamber.

Within the deposition chamber, there were several dosing lines for precursors. These included a N_2 purge line, an ATSB dosing line, an aniline dosing line, a TBS dosing line, and a TPS dosing line. These dosing lines were connected to the deposition chamber and directed toward the sample stage at a distance of 8 cm. This setup allowed for controlled delivery of the respective precursors to the sample during the process.

4.2. Deposition Process. Blanket SiO_2, blanket Si_3N_4, blanket W, and W/SiO_2 patterns were used as the substrate materials. The W/SiO_2 patterned sample was obtained from Applied Materials. The W/SiO_2 pattern has a pitch of ∼55 nm and an average line width of ∼30 nm. A barrier layer of TiN was employed between W and SiO_2. Prior to loading, all samples underwent a degreasing process using acetone, methanol, and HPLC water. Each rinse lasted approximately 10 s. After each 10 s rinse, an N_2 air gun was used to blow off any residual solution on the surface of the samples. This step was performed to ensure the complete removal of the rinsing solution. An additional 30 s 0.5% hydrofluoric acid clean followed by an HPLC water 30 s rinse was conducted only on the SiO_2 substrates.

Tris(*tert*-butoxy)aluminum (ATSB, 97%), tris(*tert*-butoxy)silanol (TBS, 99.999%), tris(*tert*-pentoxy)silanol (TPS, ≥99.99%), and aniline (ACS reagent 99.5%) were purchased from Sigma-Aldrich (ATSB, TBS, and TPS chemical structures are shown in Figure S23). Each precursor dosing line was operated with no carrier gas and had one pneumatic ALD valve and one shut-off valve. A leak valve was installed in the N_2 purge line to regulate the purging pressure. Heating tapes were employed to maintain a 150 °C uniform temperature for both the chamber wall and the dosing lines.

Prior to any CVD processes, aniline passivation was conducted by placing the samples inside the deposition chamber without pumping. The sample and aniline gas were trapped in the chamber at a temperature of 300 °C for a duration of 40 min. The passivation process was performed under a constant trapping pressure of 780 mTorr.

Previously, the ATSB pulsed CVD process was optimized at 330 °C substrate temperature for faster growth and improved selectivity.[8] The ATSB precursor bottle was heated to 110 °C. The opening time of ATSB pneumatic valve was set to 500 ms followed by a 10 s purge time between pulses which rendered a pressure spike of 0.02 mTorr. During the CVD process, a continuous flow of a N_2 purge gas was employed.

For SiO_x/AlO_x nanolaminate hybrid pulsed CVD, samples were dosed with the optimized ATSB pulses at 330 °C followed by TBS or TPS exposure (1. pulsed exposure: 500 ms opening time with 10 s purge time between pulses; 2. continuous exposure). During the experiment, the TBS bottle was kept at 88 °C while the TPS bottle was kept at 90 °C. Both TBS and TPS provide a pressure spike up to

https://doi.org/10.1021/acsami.3c13973
ACS Appl. Mater. Interfaces XXXX, XXX, XXX−XXX

1 mTorr. Various substrate temperatures were tested during the TBS exposure. Both pulsed and continuous TBS exposure modes were examined in the Results and Discussion section.

4.3. Deposition Characterization. X-ray photoelectron spectroscopy (XPS) was conducted *in vacuo* to study the as-deposited film composition in the UHV chamber. The XPS system has a monochromatic Al Kα X-ray source (E = 1487 eV) and a hemispherical analyzer (XM 1000 MkII/SPHERA, Omicrometer Nanotechnology) configured with a pass energy of 50 eV. The XPS anode voltage was set to 10 kV, and the filament emission current was set to 25 mA. All XPS data collected were analyzed by the Casa XPS v2.3 program. *Ex situ* characterization studies include atomic force microscopy (AFM), ellipsometry, transmitted electron microscopy (TEM), and electron energy loss spectroscopy (EELS).

■ ASSOCIATED CONTENT

Supporting Information

The Supporting Information is available free of charge at https://pubs.acs.org/doi/10.1021/acsami.3c13973.

> XPS showed aniline unable to passivate W against TMA dosing; raw XPS spectra of Figure 2; XPS composition analysis of the TBS reactivity test on SiN vs aniline passivated W at various substrate temperatures; reactivity study of 60 s TBS exposure on SiN and aniline passivated W at 200 °C; scatter plot and raw XPS spectra of Figure 4; scatter plot and raw XPS spectra of Figure 5; scatter plot and raw XPS spectra of Figure 6; AFM measurement of the half-supercycle hybrid pulsed CVD sample shown in Figure 5; selectivity study of half-supercycle hybrid pulsed CVD with TBS exposure at 150 °C; selectivity study of half-supercycle hybrid pulsed CVD with 120 s TBS exposure at 150 °C; selectivity study of half-supercycle hybrid pulsed CVD with 25 pulses of ATSB at 330 °C and 60 s TBS exposure at 200 °C; selectivity study of half-supercycle hybrid pulsed CVD with 100 pulses of ATSB at 330 °C and 60 s TBS exposure at 200 °C; selectivity study of half-supercycle hybrid pulsed CVD with 50 pulses of ATSB at 330 °C and 60 s TPS exposure at 150 °C; raw XPS spectra of Figure 8; electron energy loss spectroscopy (EELS) study of the W/SiO_2 patterned sample; raw XPS spectra of Figure 10a; raw XPS spectra of Figure 10c; *CV* and *IV* remeasurement of the SiO_x/AlO_x (2:1) on Si with the 25 pulses of ATSB at 330 °C and a 60 s TBS dosing at 200 °C process after 3 days left in the atmospheric condition; *CV* and *IV* remeasurement of the SiO_x/AlO_x (1:1) on Si with the 50 pulses of ATSB at 330 °C and a 60 s TBS dosing at 200 °C process after 3 days left in the atmospheric condition; *CV* and *IV* remeasurement of the SiO_x/AlO_x (2:1) on Si with the 25 pulses of ATSB at 330 °C and a 60 s TBS dosing at 200 °C process right after additional UHV 300 °C anneal; schematic diagram illustrates the custom-built ALD/CVD with the *in situ* XPS system; chemical structures from left to right: aluminum tri-*sec*-butoxide (ATSB, 97%), tris(*tert*-butoxy)silanol (TBS, 99.999%), tris(*tert*-pentoxy)silanol (TPS, ≥99.99%); selective hybrid pulsed SiO_x/AlO_x CVD on Si for capacitance study and its TEM image (PDF)

■ AUTHOR INFORMATION

Corresponding Author

Andrew Kummel − *Department of Chemistry and Biochemistry, University of California, San Diego, La Jolla, California 92093, United States;* orcid.org/0000-0001-8301-9855; Email: akummel@ucsd.edu

Authors

James Huang − *Program in Materials Science and Engineering, University of California, San Diego, La Jolla, California 92093, United States;* orcid.org/0000-0003-3279-0783

Jing Mu − *Program in Materials Science and Engineering, University of California, San Diego, La Jolla, California 92093, United States*

Yunil Cho − *Department of Electrical and Computer Engineering, University of California, San Diego, La Jolla, California 92093, United States;* orcid.org/0000-0002-2680-2015

Charles Winter − *Department of Chemistry, Wayne State University, Detroit, Michigan 48202, United States;* orcid.org/0000-0003-0416-1234

Victor Wang − *Program in Materials Science and Engineering, University of California, San Diego, La Jolla, California 92093, United States;* orcid.org/0000-0003-1544-2154

Zichen Zhang − *Program in Materials Science and Engineering, University of California, San Diego, La Jolla, California 92093, United States;* orcid.org/0000-0001-8028-3271

Kesong Wang − *Department of Mechanical and Aerospace Engineering, University of California, San Diego, La Jolla, California 92093, United States*

Chanyoung Kim − *Department of Nanoengineering, University of California, San Diego, La Jolla, California 92093, United States;* orcid.org/0000-0003-2749-8163

Ajay Yadav − *Applied Materials, Inc., Santa Clara, California 95054, United States*

Keith Wong − *Applied Materials, Inc., Santa Clara, California 95054, United States*

Srinivas Nemani − *Applied Materials, Inc., Santa Clara, California 95054, United States*

Ellie Yieh − *Applied Materials, Inc., Santa Clara, California 95054, United States*

Complete contact information is available at: https://pubs.acs.org/10.1021/acsami.3c13973

Notes

The authors declare the following competing financial interest(s): The UCSD team was funded by Applied Materials for this research; Applied Materials scientists are included as coauthors on this manuscript. However, there is no direct link to product production since the manuscript is focused on process chemistry and Applied Materials makes process equipment not process chemical.

■ ACKNOWLEDGMENTS

Funding support from Applied Materials is gratefully acknowledged. The ellipsometry measurements were facilitated by the San Diego Nanotechnology Infrastructure (SDNI), which is supported by the National Science Foundation (NSF) to Nano3 (Grant ECCS-1542148).

REFERENCES

(1) Chen, H.; Wu, Y.; Huang, H.; Tsai, C.; Lee, S.; Lee, C.; Wei, T.; Yao, H.; Wang, Y.; Liao, C.; Chang, H.; Lu, C.; Shue, W.; Cao, M. Fully Self-Aligned Via Integration for Interconnect Scaling Beyond 3nm Node. *2021 IEEE International Electron Devices Meeting (IEDM)* **2021**, 22.1.1−22.1.4.

(2) Hashemi, S. M.; Prasittichai, C.; Bent, S. A New Resist for Area Selective Atomic and Molecular Layer Deposition on Metal−Dielectric Patterns. *J. Phys. Chem. C* **2014**, *118* (20), 10957−10962.

(3) Pasquali, M.; Gendt, S. D.; Armini, S. Area-Selective Deposition by A Combination of Organic Film Passivation and Atomic Layer Deposition. *ECS Trans.* **2019**, *92* (3), 25−32.

(4) Liu, T. L.; Nardi, K. L.; Draeger, N.; Hausmann, D. M.; Bent, S. Effect of Multilayer Versus Monolayer Dodecanethiol on Selectivity and Pattern Integrity in Area-Selective Atomic Layer Deposition. *ACS Appl. Mater. Interfaces* **2020**, *12* (37), 42226−42235.

(5) Shearer, A.; Bent, S.. Area-Selective Atomic Layer Deposition Using Nitrogenous Aromatic Small Molecule Inhibitors. **2022**, *ASD2022*.

(6) Merkx, M. J. M.; Vlaanderen, S.; Faraz, T.; Verheijen, M. A.; Kessels, W. M. M.; MacKus, A. J. M. Area-Selective Atomic Layer Deposition of TiN Using Aromatic Inhibitor Molecules for Metal/Dielectric Selectivity. *Chem. Mater.* **2020**, *32* (18), 7788−7795.

(7) Oszinda, T.; Schaller, M.; Schulz, S. E. Chemical Repair of Plasma Damaged Porous Ultra Low-K SiOCH Film Using a Vapor Phase Process. *J. Electrochem. Soc.* **2010**, *157* (12), H1140.

(8) Huang, J.; Cho, Y.; Wang, V.; Zhang, Z.; Mu, J.; Yadav, A.; Wong, K.; Nemani, S.; Yieh, E.; Andrew, K. Dielectric-on-Dielectric Achieved on SiO_2 in Preference to W by Water-free Chemical Vapor Depositions with Aniline Passivation. *ACS Applied Materials & Interfaces* **2023**, *15* (21), 26128−26137.

(9) Cho, Y.; Huang, J.; Zhang, Z.; Wang, K.; Lee, P.; Kim, C.; Wong, K.; Nemani, S.; Yieh, E.; Kummel, A. C. Inherent Selective Pulsed Chemical Vapor Deposition of Aluminum Oxide in nm Scale. *Appl. Surf. Sci.* **2023**, *622*, No. 156824.

(10) Cho, Y.; Ahles, C. F.; Choi, J. Y.; Huang, J.; Jan, A.; Wong, K.; Nemani, S.; Yieh, E.; Kummel, A. C. Inherently Selective Water-Free Deposition of Titanium Dioxide on the Nanoscale: Implications for Nanoscale Patterning. *ACS Appl. Nano Mater.* **2022**, *5* (1), 476−485.

(11) Huang, J.; Cho, Y.; Zhang, Z.; Jan, A.; Wong, K. T.; Nemani, S. D.; Yieh, E.; Kummel, A. C. Selective Pulsed Chemical Vapor Deposition of Water-Free TiO_2/Al2O3 and HfO2/Al2O3 Nanolaminates on Si and SiO_2 in Preference to SiCOH. *ACS Appl. Mater. Interfaces* **2022**, *14* (13), 15716−15727.

(12) Ovanesyan, R. A.; Filatova, E. A.; Elliott, S. D.; Hausmann, D. M.; Smith, D. C.; Agarwal, S. Atomic Layer Deposition of Silicon-Based Dielectrics for Semiconductor Manufacturing: Current Status and Future Outlook. *Journal of Vacuum Science & Technology A* **2019**, *37* (6), No. 060904.

(13) Han, B.; Zhang, Q.; Wu, J.; Han, B.; Karwacki, E. J.; Derecskei, A.; Xiao, M.; Lei, X.; O'Neill, M. L.; Cheng, H. On the Mechanisms of SiO_2 Thin-Film Growth by the Full Atomic Layer Deposition Process Using Bis(t-butylamino)silane on the Hydroxylated SiO_2 (001) Surface. *J. Phys. Chem. C* **2012**, *116* (1), 947−952.

(14) Fang, G.; Xu, L.; Ma, J.; Li, A. Theoretical Understanding of the Reaction Mechanism of SiO_2 Atomic Layer Deposition. *Chem. Mater.* **2016**, *28* (5), 1247−1255.

(15) Kim, D. H.; Lee, H. J.; Jeong, H.; Shong, B.; Kim, W. H.; Park, T. J. Thermal Atomic Layer Deposition of Device-Quality SiO_2 Thin Films under 100 °C Using an Aminodisilane Precursor. *Chem. Mater.* **2019**, *31* (15), 5502−5508.

(16) Choi, D.; Kim, B. K.; Chung, K. B.; Park, J. S. Studies on Optical, Chemical, and Electrical Properties of Rapid SiO_2 Atomic Layer Deposition Using Tris(tert-butoxy)silanol and Trimethyl-aluminum. *Mater. Res. Bull.* **2012**, *47* (10), 3004−3007.

(17) Choi, D. W.; Chung, K. B.; Park, J. S. Rapid Vapor Deposition SiO_2 Thin Film Deposited at a Low Temperature Using Tris(tert-pentoxy)silanol and Trimethyl-aluminum. *Mater. Chem. Phys.* **2013**, *142* (2−3), 614−618.

(18) Burton, B. B.; Boleslawski, M. P.; Desombre, A. T.; George, S. M. Rapid SiO_2 Atomic Layer Deposition Using Tris(tert-pentoxy)-silanol. *Chem. Mater.* **2008**, *20* (22), 7031−7043.

(19) Fang, G.; Ma, J. Rapid Atomic Layer Deposition of Silica Nanolaminates: Synergistic Catalysis of Lewis/Brønsted Acid Sites and Interfacial Interactions. *Nanoscale* **2013**, *5* (23), 11856−11869.

(20) Won, S. J.; Kim, J. R.; Suh, S.; Lee, N. I.; Hwang, C. S.; Kim, H. J. Effect of Catalyst Layer Density and Growth Temperature in Rapid Atomic Layer Deposition of Silica Using Tris(tert-pentoxy)silanol. *ACS Appl. Mater. Interfaces* **2011**, *3* (5), 1633−1639.

(21) Tezsevin, I.; Maas, J. F. W.; Merkx, M. J. M.; Lengers, R.; Kessels, W. M. M.; Sandoval, T. E.; Mackus, A. J. M. Computational Investigation of Precursor Blocking during Area-Selective Atomic Layer Deposition Using Aniline as a Small-Molecule Inhibitor. *Langmuir* **2023**, *39* (12), 4265−4273.

(22) Leung, K.; Nielsen, I. M. B.; Criscenti, L. J. Elucidating the Bimodal Acid−Base Behavior of the Water−Silica Interface from First Principles. *J. Am. Chem. Soc.* **2009**, *131* (51), 18358−18365.

(23) Ballinger, P.; Long, F. A. Acid Ionization Constants of Alcohols. II. Acidities of Some Substituted Methanols and Related Compounds1,2. *J. Am. Chem. Soc.* **1960**, *82* (4), 795−798.

(24) Lingane, J. Treatise on Analytical Chemistry. Volume 1 of Part 1, Theory and Practice (Kolthoff, I. M.; Elving, Philip J.; Sandell, Ernest B.; eds.). *J. Chem. Educ.* **1960**, *37* (2), 108.

(25) Clark, A. Principles of Chemistry. Third edition (Hildebrand, Joel H.). *J. Chem. Educ.* **1932**, *9* (8), 1495.

https://doi.org/10.1021/acsami.3c13973
ACS Appl. Mater. Interfaces XXXX, XXX, XXX−XXX